



## Numerical Study on the Behaviour of Built-up Cold-Formed Steel Corrugated Web Beams End Connections

Ioan Both <sup>1</sup>, Mircea Burca <sup>1</sup>, Stefan Benzar <sup>1</sup>, Viorel Ungureanu <sup>1, 2\*</sup>

<sup>1</sup> Politehnica University of Timisoara, Str. Ioan Curea, No. 1, Timisoara 300224, Romania.

<sup>2</sup> Romanian Academy, Blvd. Mihai Viteazu, No. 24, Timisoara 300223, Romania.

Received 17 January 2023; Revised 12 March 2023; Accepted 23 March 2023; Published 01 April 2023

### Abstract

Corrugated web beams made of cold-formed steel components represent an economical solution for structures, offering high flexural capacity and deformation rigidity. For conventional corrugated web beams, made of thick plates for the flanges and thin sinusoidal steel sheets for the web, the elements can be joined by standard bolted end-plate connections. In the case of corrugated web beams made of thin-walled cold-formed steel components only, additional plates are required to accommodate the shape and position of the profiles. A large experimental program was carried out on corrugated web beams made of cold-formed steel elements. One of the objectives was to determine the capacity of these beams and the influence of several parameters on the response of the beam, but also very important were the end connections of these beams. The recordings obtained from the tests were used to validate a numerical model. Based on the validation of the numerical model, finite element analyses were performed to study four solutions for end connections to facilitate assembly, optimise the number of bolts, and increase the capacity and rigidity. Although the connection can be improved for assembling reasons with the presented solutions, the overall capacity is limited by the components subjected to compression that lose their stability.

*Keywords:* Cold-Formed Steel; Corrugated Web Beams; End Connections; Experimental Tests; Finite Element Analyses.

### 1. Introduction

Reducing material consumption without affecting the required performance of structural elements is of main interest in structural design optimisation. New solutions are recently studied, for example, cold-formed steel box girders with flanges of the C-section and sinusoidal corrugated sheets [1], cold-formed steel box girders with tubular flanges and sinusoidal corrugated sheets [2], cold-formed steel back-to-back connected built-up beams [3], cold-formed steel beams of corrugated sheet and built-up section for flanges, [4], lightweight composite floor system: cold-formed steel and concrete [5], cold-formed steel trusses using mechanical clinching [6], cold-formed steel trusses with semi-rigid joints [7], cold-formed steel hollow beam with perforation [8], wood composite I-beams with sinusoidal corrugated web [9].

As observed, web corrugation leads to a significant number of structural solutions because of the important material savings. The classical solution for connections is the bolted connection. The response of such connections can be determined using the provisions of the component method given in [10]. Another classical type of connection, generally used, is with high-strength preload bolts, according to EN 14399 [11]. Nevertheless, practice shows that the costs of preload bolts are three times the costs of non-preload bolts. Since cold-formed elements use smaller diameters of bolts, not necessarily of high strength, the final costs of the joint can be reduced. However, it is known from the literature that cold-formed steel connections have semi-rigid behaviour [12].

\* Corresponding author: [viorel.ungureanu@upt.ro](mailto:viorel.ungureanu@upt.ro)

<http://dx.doi.org/10.28991/CEJ-2023-09-04-01>



© 2023 by the authors. Licensee C.E.J, Tehran, Iran. This article is an open access article distributed under the terms and conditions of the Creative Commons Attribution (CC-BY) license (<http://creativecommons.org/licenses/by/4.0/>).

The capacity of the classical case of moment connection for cold-formed steel by bolting the web to the stiffened gusset plate is limited by the local buckling of the web adjacent to the connection [13]. For the combined action, Mojtabaei et al. [13] concluded that a linear equation accurately captures the interaction between the bending moment and the axial force, while the effects of a shear force less than half of the shear capacity on the bending moment capacity can be neglected. Papargyriou et al. [14] developed two connection configurations that engage the flanges of the profiles. Compared to the web-connected joint, the two new configurations in which either the flanges are connected or both the flange and the web are connected in the joints lead to higher flexural capacity although the rotation capacity is smaller if stiffened angle sections are used for the flanges.

Ye et al. [15] demonstrated improved behaviour of the connections for cold-formed steel bolted connection, considering the friction-slip mechanism which increases the ductility by up to 200% and improves the cyclic response of the CFS connections. Fahmy et al. [16] investigated the structural behaviour of cold-formed steel beam-column connections. Experimental tests on five specimens and FE analyses for frame connections have been studied using new configurations of beam-column connections such as gusset plates and self-drilling screws. They proposed some recommendations for choosing the optimal type of beam-to-column connection. Hanna et al. [17] performed experimental and numerical investigations on the behaviour of beam-to-column single lipped channel cold-formed section screw fastened connections subjected to major axis bending moments using tapered gusset plates and also rectangle ones. They found that specimens with a tapered gusset plate reach about 80% of the beam section flexural capacity, while for specimens with a rectangular gusset plate this ratio becomes 60%.

Sabbagh et al. [18] investigated the cyclic behaviour of the cold-formed steel semi-rigid moment-resisting connection filled with rubberized concrete for seismic application. The tests were carried out on bare steel and composite connections under cyclic loading. The results showed that the composite connection typically reaches 45% higher strength and 21% higher energy dissipation capacity than the bare steel connection. Nagy et al. [19] studied the behaviour of back-to-back cold-formed lipped channel beams-to-SHS column joints under monotonic and cyclic loading. An experimental program was carried out on two different configurations in order to evaluate the structural performance of such joints for low-rise multi-storey steel framed structures. They found that the analysed joints produced excessive rotation, and for such a structure it is recommended to always use a braced structural configuration.

Rinchen & Rasmussen [20] investigated the behaviour of connections of cold-formed steel portal frames with single C-section members through the combination of laboratory tests and finite element analyses. The main objective was to establish moment-rotation characteristics and to derive flexural stiffness values. Simplified multi-linear in-plane bending moment-rotation relations and the corresponding flexural stiffness values were derived for the eaves, apex and base connections. These relations can be used to represent the semi-rigidity of the connections when modelling the investigated cold-formed steel portal frames with beam elements. Bondok & Salim [21] investigated the failure capacities and the energy absorption capacities of the end-connections of the roof truss. 24 experimental tests on connections, with symmetric and non-symmetric conditions, have been performed to determine the capacities and failure modes of the end-connections for cold-formed steel trusses under horizontal (shear) and vertical (tension) loads. Numerical simulations were developed to predict the response to failure of the connection for any configuration. The results showed that the toughness (energy absorbed to failure) of the end connection is greatly affected by the screw configuration and the direction of loading.

Lukačević et al. [22] investigated an innovative fabricated angle bracket connection to join cold-formed steel structures. This angle bracket can be used to connect cold-formed steel elements such as beam trusses at the ends of the chords or to anchor the column base. They found that the main failure mechanism of the angle bracket connection determined by experimental tests was pull-through of the bolt and no bearing failure in the connection between the C-profile and the angle bracket, which indicates an increase in the bearing capacity of the connection. Deng et al. [23] proposed a connection for modular steel construction as a fully prefabricated liftable connection with compressive resistance closely related to the thickness, length, and strength of the module column. Lacey et al. [24] conducted a review of intermodule interconnects in modular steel buildings where three specific connections were discussed and highlighted that existing studies consider a single load action and not combined actions. In cases where combined actions have been applied, it is difficult to separate the response into individual components.

A new hybrid modular construction system was developed within the European project INNO3DJOINTS [25] aiming to develop innovative plug-and-play joints that enable modularity, faster construction and deconstruction. The proposed system is made of light-weight steel truss connected with plug-and-play joints to tubular columns. A parametric study was carried out that compared the 2D and 3D structural behaviour of the proposed system with that of conventional steel solutions [26]. The parameters examined were the type of truss, the variation in the span, the lateral force resisting system, and the type of floor system. Improvements in joints for efficient structural parts also represent a research interest. The study by Simões da Silva et al. [27] showed the efficiency of innovative plug-and-play joints for lightweight truss beams in low seismicity zones.

It can be concluded that there is a lack of knowledge on the best practises and connection techniques of corrugated web beams (CWBs) in the literature, lacking information on alternative connection geometries, fast assembling, or optimisation of the parts engaged in the force distribution.

The paper presents an experimental study of corrugated web beams with an emphasis on the response of the beam connections. The response is characterised by slippages and deformations between the parts of the beam and the end plate. A finite element model is validated for the entire beam using shell elements, while for the beam end, solid elements were used in a separate model. After validation of the numerical model based on experimental data and material properties, four solutions are presented to allow fast assembly and provide reliable resistance and stiffness of the connection. The proposed solutions can reduce assembly time, but the capacity and rigidity are limited by the instability of the compressed parts.

## 2. Materials and Methods

### 2.1. Experimental Data

#### 2.1.1. Corrugated Web Beams

The material distribution in corrugated web beams is very efficient because of the small thickness of the web. The stability of the web is provided by the corrugations, which reduce the flat area, which is susceptible to buckling.

Two corrugated web beams were built-up using spot welding (noted with SW1 and SW2 in the following) and three corrugated web beams were built-up using MIG (Metal Inert Gas) brazing (noted with CMT1, CMT2, and CMT3) [28, 29]. Particular to the built-up cold-formed corrugated web beams are the 1) shear panels (also thin flat sheets), 2) the trapezoidal corrugated sheets and 3) the lipped C-sections, while supplementary reinforcing profiles, 4), under the load application points were provided for the tested specimens, as presented in Figure 1.

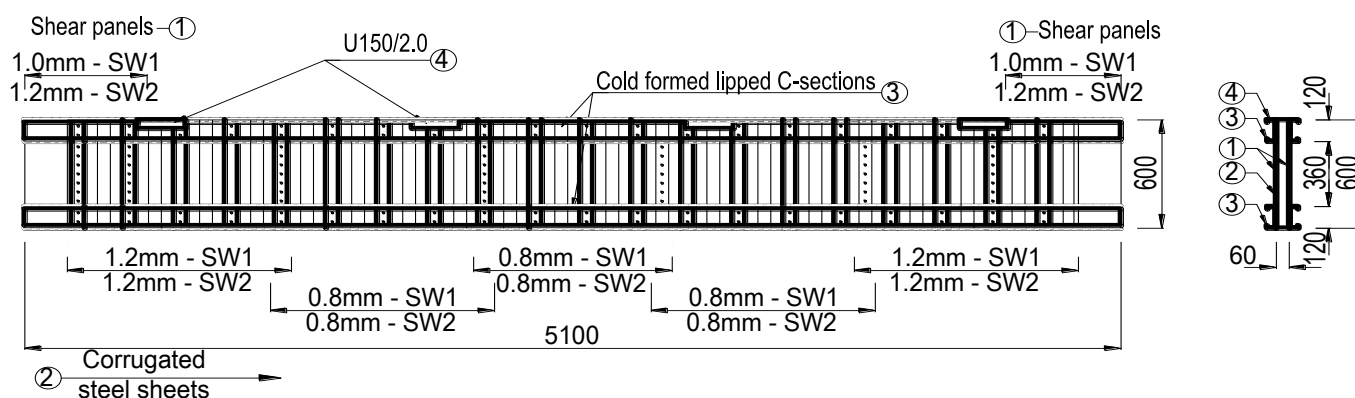


Figure 1. Components of the built-up corrugated web beams

The thicknesses presented in Figure 1 relate to the steel sheets used for the beams connected by spot welding. The shape of the lipped C-section follows the height of 120 mm, the width of 60 mm and the lip of 20 mm with a thickness of 2.0 mm.

The beam was designed to be tested in a six-point bending configuration using the test setup presented in Figure 2. Support devices were designed to fit the rigid frame element position, as presented in Section 2.1.2. The four loading points were positioned at distances of  $L/8 : L/4 : L/4 : L/8$ . A separate structure was assembled to prevent out-of-plane deformation of the beam, the contact between the beam and the secondary structure being provided by greased Teflon pads, fixed on steel parts bolted to the top flange of the CWB beam. An actuator was used to load the beam through a leverage system. The beams of the leverage system came into contact with the CWB beam through the 80 mm cylinders placed on steel plates to distribute the point load and further to the U150/2 parts, to prevent stress concentrations.

Vertical deflections were recorded for the beam, while horizontal transducers were used for the behaviour of the connections. Two wire displacement transducers were placed at each quarter of the beam, monitoring each C-section of the bottom flange (see Figure 3). The monitoring of the connection is discussed in Section 2.1.2.

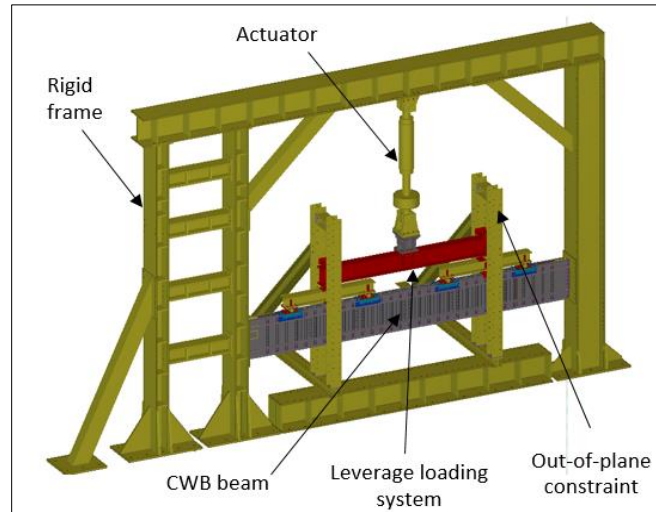


Figure 2. Test setup for CWB beams

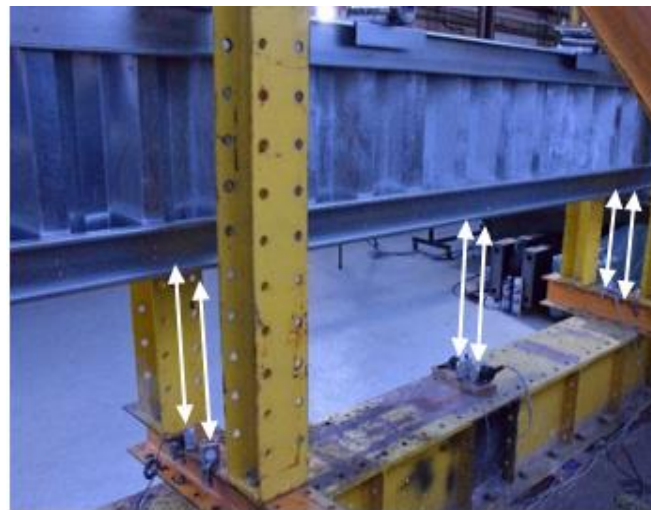


Figure 3. Vertical deflection measurement positions

**2.1.2. Connections**

Although several types of connections are used to assemble the CWB beams (see Figure 4-a), the interest of this study is represented by the bolted connection at the end of the beams, with adjacent elements, i.e. positions (4) and (5) in Figure 4-a. Nevertheless, few details are also given for the connections between the parts of the CWB.

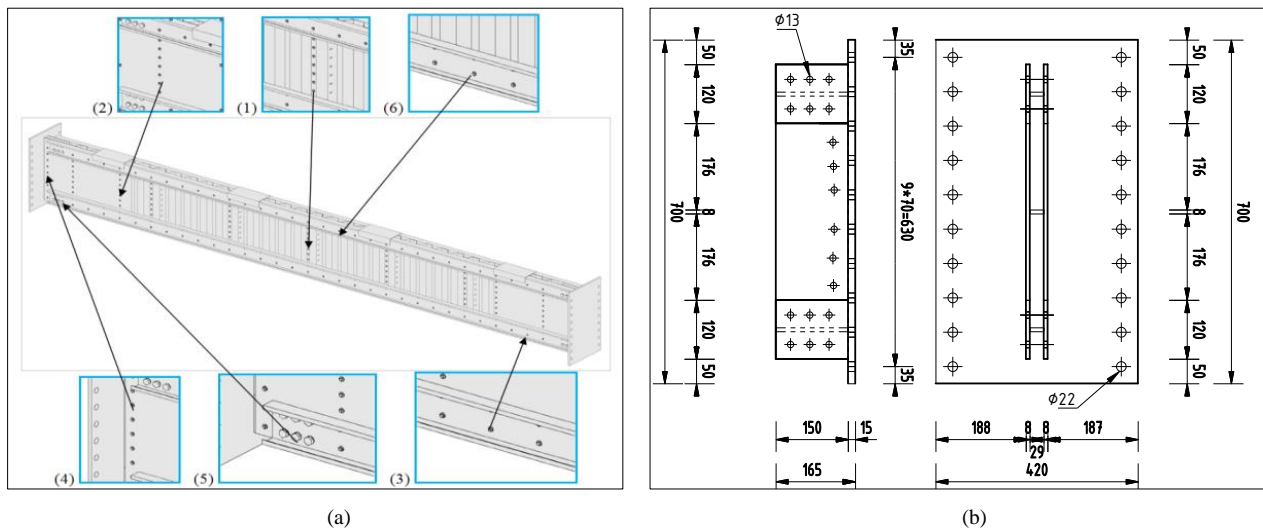


Figure 4. a) Connections of the corrugated web beam, b) Support device assembly (SDA)

As mentioned, spot welding [28] and MIG brazing [29] were two efficient techniques to join the thin cold-formed parts of the beam. For each case of joining, shear lap specimens (see Figure 5), of different sheet thicknesses, were tested to determine the response of the connections between the parts of the beam.

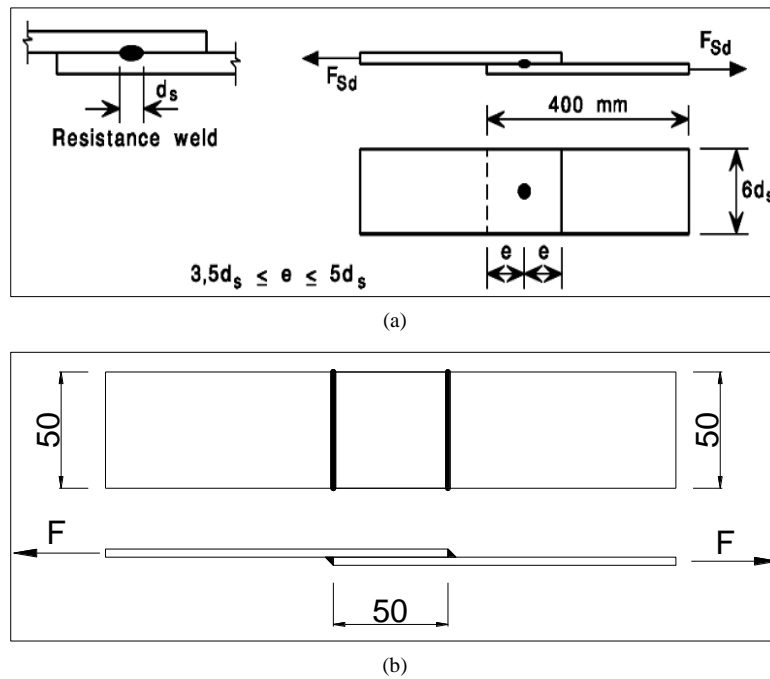


Figure 5. Shear lap joint specimens a) spot welded [28], b) MIG brazed [29]

The SW specimen consisted of one spot weld, whereas the MIG brazed specimen joined the two sheets by two throats. All brazed specimens had the same width, while the sheet width of spot-welded specimens depended on the nominal size of the welding nugget, which also depends on the thickness of the steel sheets. A flange end-plate assembly SDA was designed to fix the beam ends to the rigid testing frame. The end-plates were 15 mm thick, while the fins were made of 8 mm steel plates (see Figure 4-b). The end-plates had 22 mm holes, for M20 grade 10.9 bolts, to connect the SDA assembly to the rigid testing frame, while the cold-formed steel parts (flanges and shear panels) and the 8 mm fins were designed with 13 mm holes, for the M12 grade 8.8 bolts, to connect the SDA assemblies to the beam, as presented in Figure 4-a.

The response of the bolted connection was determined using displacement transducers. Two transducers were fixed on each C-profile, at the last bolt position, to determine the slippage between the flanges and the 8 mm plates of the support device. The transducer monitored slippage with respect to the end-plate through the rod connecting the fixation point and the end of the rod. A displacement transducer was fixed only at the top flange to monitor the deformation of the end-plate due to bending. The transducer was fixed on the 8 mm fins and recorded the deformation with respect to the rigid frame. As the tension develops only in the top flange, the deformation of the end-plate was not monitored at the bottom flange. The position of the transducers is shown in Figure 6.

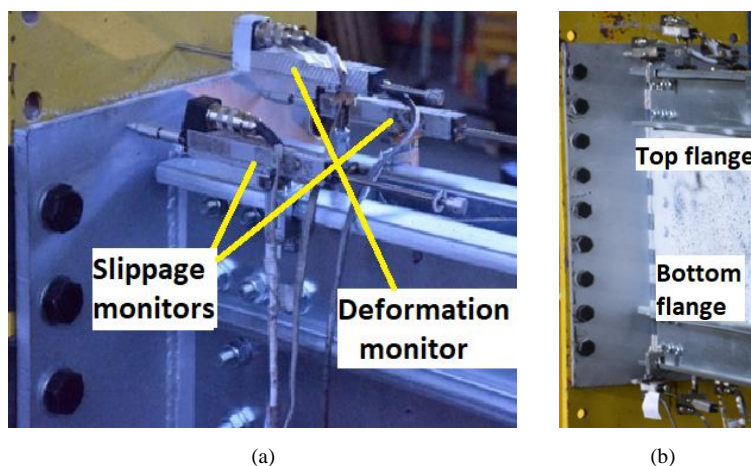


Figure 6. a) Deformation and slippage measurements for top flange, b) 3 LVDTs for top flange, 2 LVDTs for bottom flange

**2.1.3. Base Material**

The material properties for all steel sheet thicknesses were determined according to ISO 6892-1 [30]. The tests were performed on non-proportional specimens with parallel sides, a width of 20 mm, and a gauge length of 80 mm. Experimental tests were carried out using the universal UTS testing machine with a contact extensometer and a capacity of 250 kN [28, 29].

**2.2. Finite Element Model**

The stress concentration in the connection is difficult to monitor experimentally. Numerical analyses were performed for full-scale beam specimens using Abaqus v. 6.14 [31]. The built-up beam parts were defined as extruded 3D shell elements according to the shape of the part. An approximate global size of 15 mm was set for the definition of the element dimensions. The type of finite element S4R, doubly curved thin or thick shell with 4-node, reduced integration, hourglass control and finite membrane strains were selected for the calculation considerations. The material models for all parts of the built-up beams were defined considering the results of the tensile tests performed on the base material presented in Section 3.1.3 and transformed into the True-Stress-Strain relations according to EN1993-1-5, Annex C [32]. Although the support conditions were defined on the nodes of the holes provided for the bolts that connect the beam to the end-plate assembly as null displacements and rotations (see Figure 7-b), the loading of the beam was defined as a vertical displacement in a set of multipoint constraints MPC that forms a leverage system to transmit the deflection to the four loading points, as Figure 7-a presents.



**Figure 7. a) FEM model of the beam, b) support boundary condition**

For this model, due to the multitude of contact areas, the *All\*with self*-option was used for the interaction between parts with a *Penalty formulation* of 0.1 *Friction Coefficient*, for the tangential behaviour and *Hard* contact for the normal behaviour. The spot welds were defined as *Attachment points* on each part where the spot welding was applied. The connection between the attachment points was defined using *Point Based Fasteners* with the *Connector* response of the spot welding initially calibrated from the tensile-shear tests results. The connector was considered by the *Elasticity*, *Plasticity*, *Damage* and *Failure* parameters. For detailed monitoring of the connection, a 3D model using solid elements was defined. Model parts, i.e. bolts, lipped C profile, shear panel, steel plate for flange, and steel plate for web are presented in Figure 8. To avoid conflicts due to the large number of constraints in the 3D model, friction was defined in *surface pairs*.

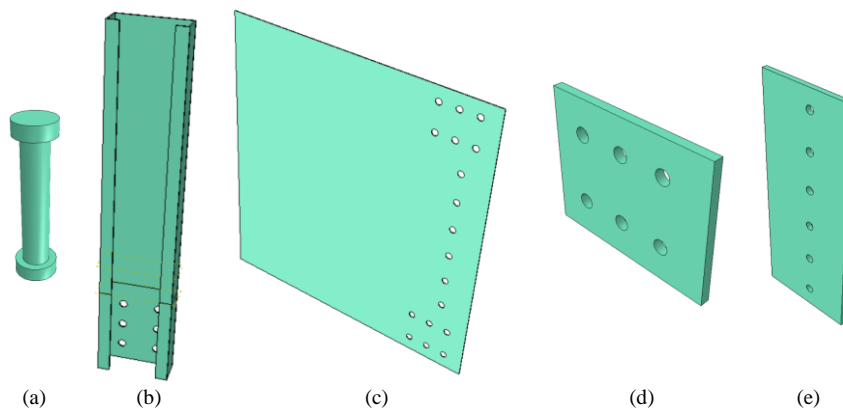


**Figure 8. Defined parts of the finite element model: a) bolts, b) lipped C-profile, c) shear panel,**

For the thin gauge defined parts, true stress-strain material curves were defined from the tensile tests, while for the support parts, the nominal yield limit of 355 MPa and for the bolts, elastic behaviour, were defined respectively. The elements mesh size for the bolt was set to 2 mm while the elements for the lipped channels had a decreasing size along the part with the minimum size of 4 mm in the connection area. A rigid body constraint was defined for the steel plate supports restraining all 6 DOFs. To uniformly apply the load, a coupling constraint enabling all DOFs was defined for all four lipped channels cross-section. As the results will be compared to the brazed specimens, the parts were connected using the *Tie* constraint. The numerical analysis consists of two steps i.e. the Frequency step for the initial imperfections (equivalent with the thickness of the steel sheet) and the dynamic, explicit step used to run the load-displacement analysis of the beam based on geometry from the first static analysis and with all contacts and material nonlinearity included. The assembly of parts for the beam end connections, the constraints, the applied mesh and the considered initial imperfections are presented in Figure 9.

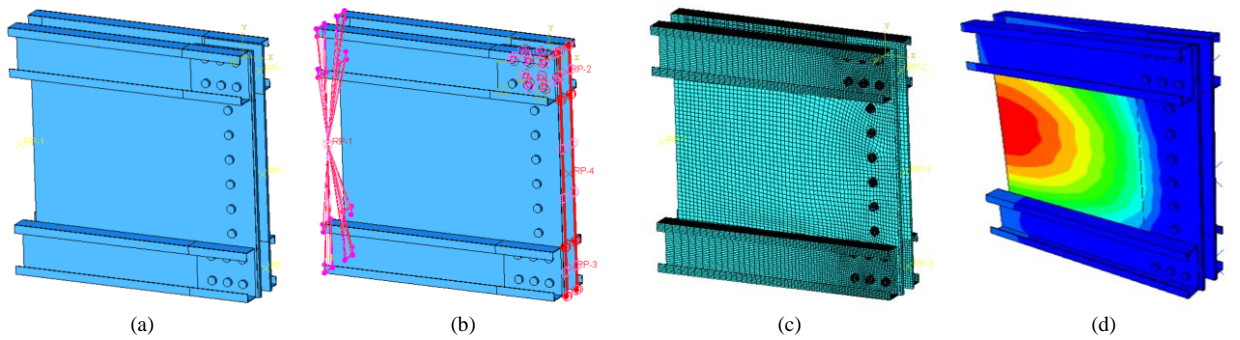


Figure 9. a) Assembly of the connection, b) Constraints, c) Finite elements mesh, d) initial imperfection

The analysis considerations are similar to the ones presented above, but the loading was applied in the control point connected to the surface of the lipped channel profile cross-section. The steel plates for the flange and the web were not connected, to allow separate assessment of the force in the flange and in the web.

### 3. Results

#### 3.1. Experimental Data

##### 3.1.1. Corrugated Web Beams

The response of the full-scale beams presents different values for both resistance and rigidity depending on the parts joining technique, i.e. spot welding or MIG brazing. From the force vs. mid-span deflection curves (see Figure 10), an increased rigidity is observed for the MIG brazed specimen, compared to the SW beams. Between the discrete connection of the spot welding and the relatively long brazed throats, the MIG brazing offers increased stability for thin steel sheets. This stabilising effect leads to increased resistance, although the maximum force applied to the SW specimens is limited by the relatively regular force drops, which represent failure of the spot weld joints between the corrugated steel sheets and the C profiles, mostly nugget pull-out type of failure.

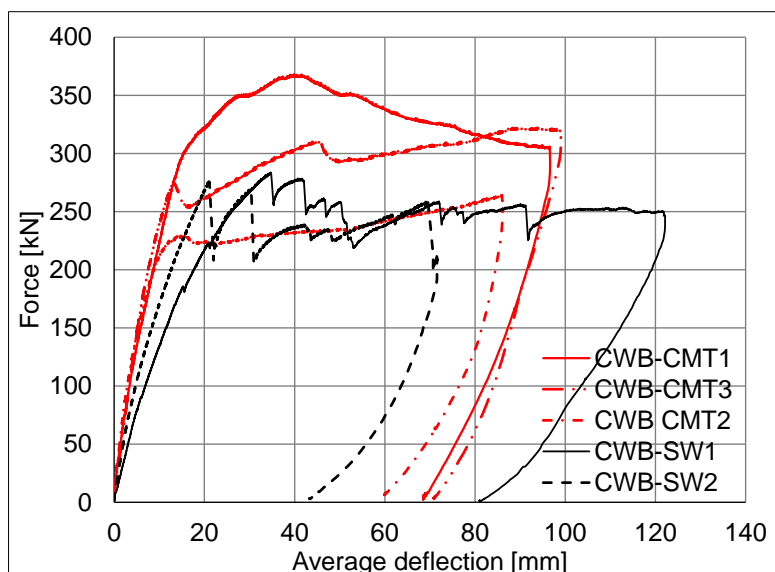


Figure 10. Force-deflection curves of the corrugated web beams

### 3.1.2. Connections

The response of the beams is influenced by the response of the connection between the beam parts. For the lap joint specimens connected by spot-welding, the test pieces have smaller capacity due to the smaller connecting surface and the failure mode. The spot-welded specimens allowed the separation of connected pieces, also involving bending stresses, while the deformation of the MIG brazed specimens is more compact (see Figure 11).

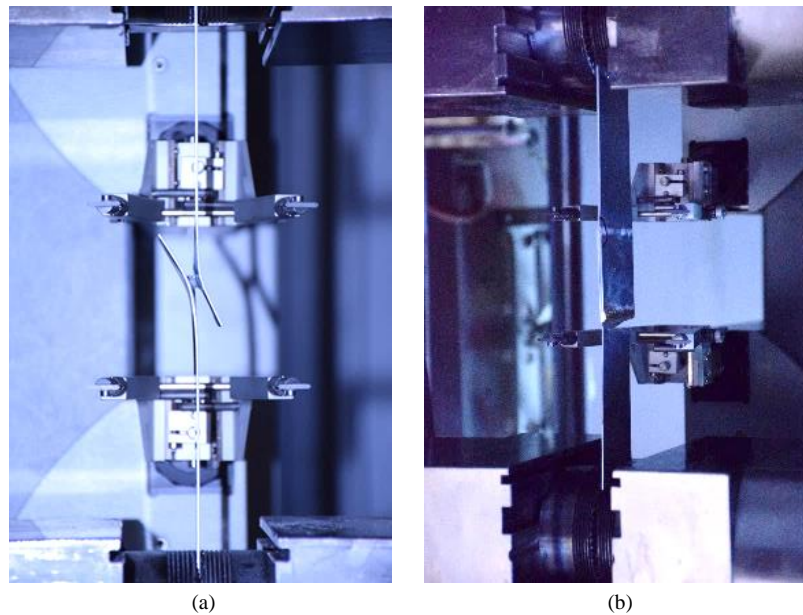


Figure 11. Deformation of the tested shear lap joint specimens a) spot welded, b) MIG brazed

Regarding the capacity of each combination of sheet thicknesses, the maximum force resisted by the spot-welded specimens depends on the nugget size, which also depends on the sheet thickness joined, thus increasing the resistance function of the combined sheet thicknesses (see Figure 12-a). For the same sheet thickness joined with different sheet thicknesses by MIG brazing, the maximum force is similar, showing that the limitation is given by the material properties and not by the brazing process, as shown in Figure 12-b for steel sheets of 1.5 mm joined with steel sheets of 1.5, 2.0, 2.5 mm.

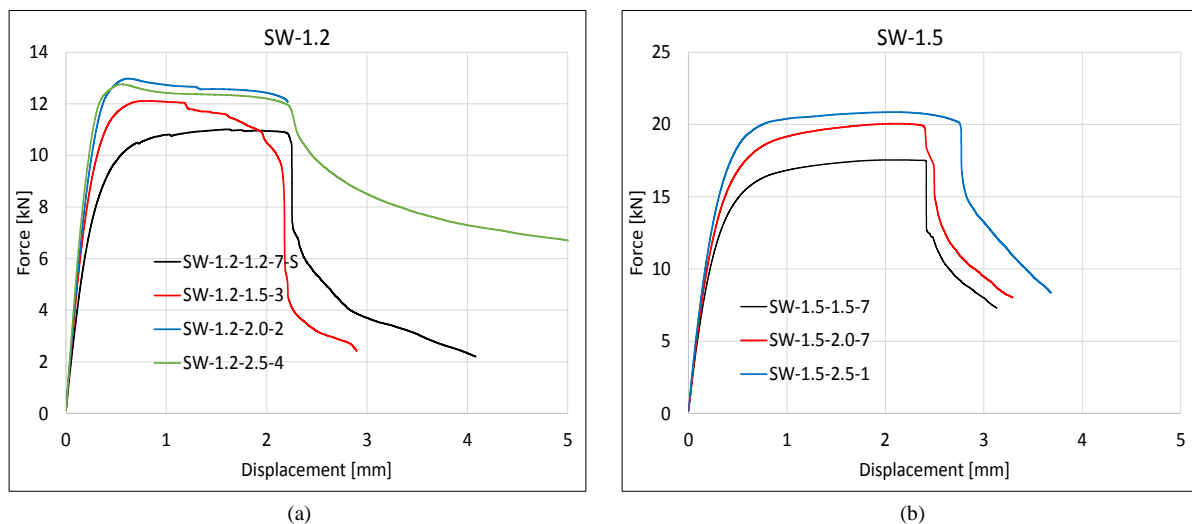


Figure 12. Resistance of the shear lap joint behaviour a) spot welded, b) MIG brazed

Figure 13 presents the response of the end plate of the support assembly to assess the influence of the connection on the overall response of the beam. The left support device presents a similar initial rigidity for all beams, but, due to the larger capacity of CMT-1, the end plate reached its plasticity. A similar plastic response can be observed for the right support of CMT-1, but with a larger value. Plastic deformations are also observed for the SW beams and CMT-3. These plastic deformations of the SW and CMT-3 beams occurred after reaching the maximum force of each beam. The force value is determined from the bending moment calculated for the CWB in the supports of the beam, divided by the lever arm between the upper and lower flange axes.

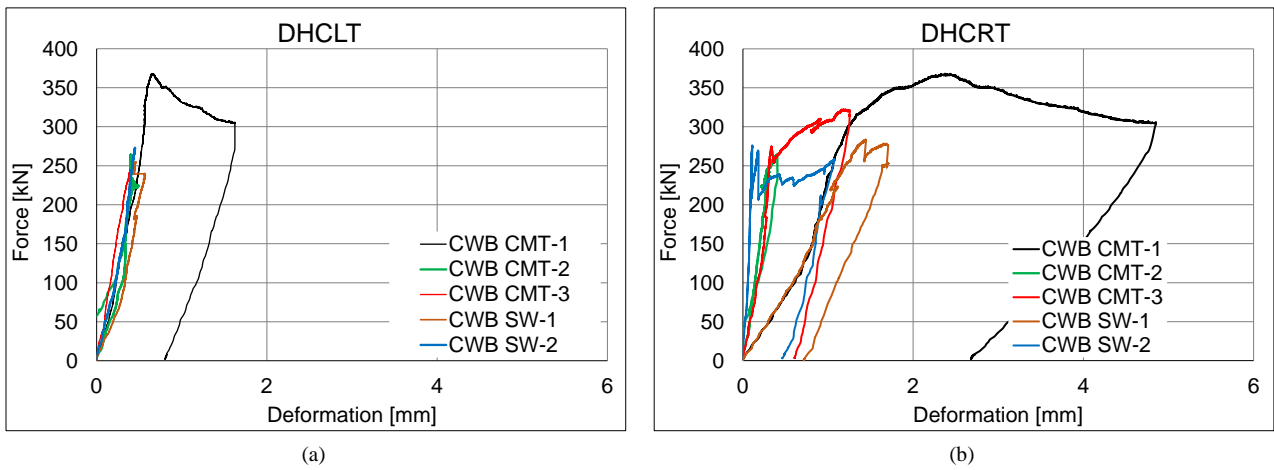


Figure 13. Deformation of the end plates: a) left side, b) right side

The response of the connections between the flanges and the plates of the support device are presented in Figures 14 to 17. For the bottom connection (see Figures 14 and 15) slightly higher values of deformation are observed between the left- and right-hand connections. This phenomenon occurred for both visible parts of the beam (1) and for the backward parts of the beam (2) in the case of CMT beams. The deformation of the SW beam connections presents similar elastic deformation and similar deformation values for the left and right connections.

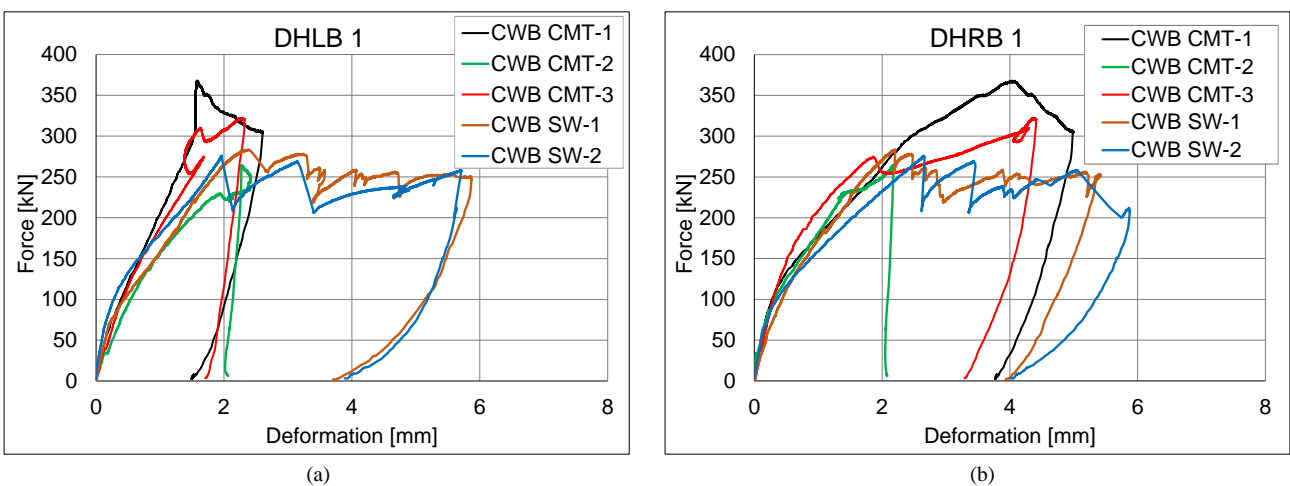


Figure 14. Slippages and deformations of the frontal bottom connection between the flanges and the support:-a) left side, b) right side

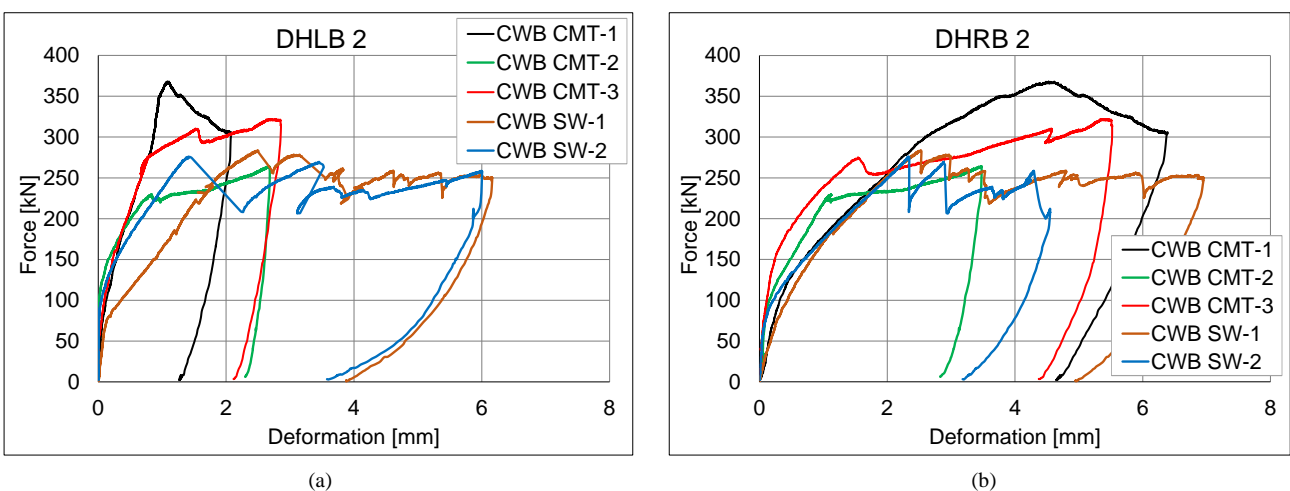


Figure 15. Slippages and deformations of the backward bottom connection between the flanges and the support: a) left side, b) right side

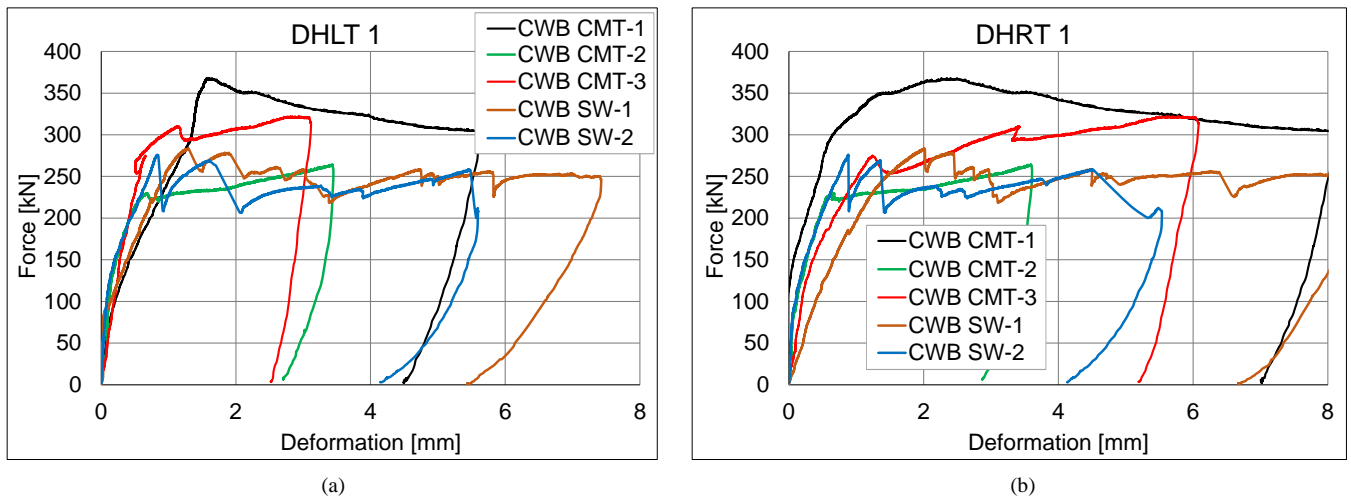


Figure 16. Slippages and deformations of the frontal top connection between the flanges and the support: a) left side, b) right side

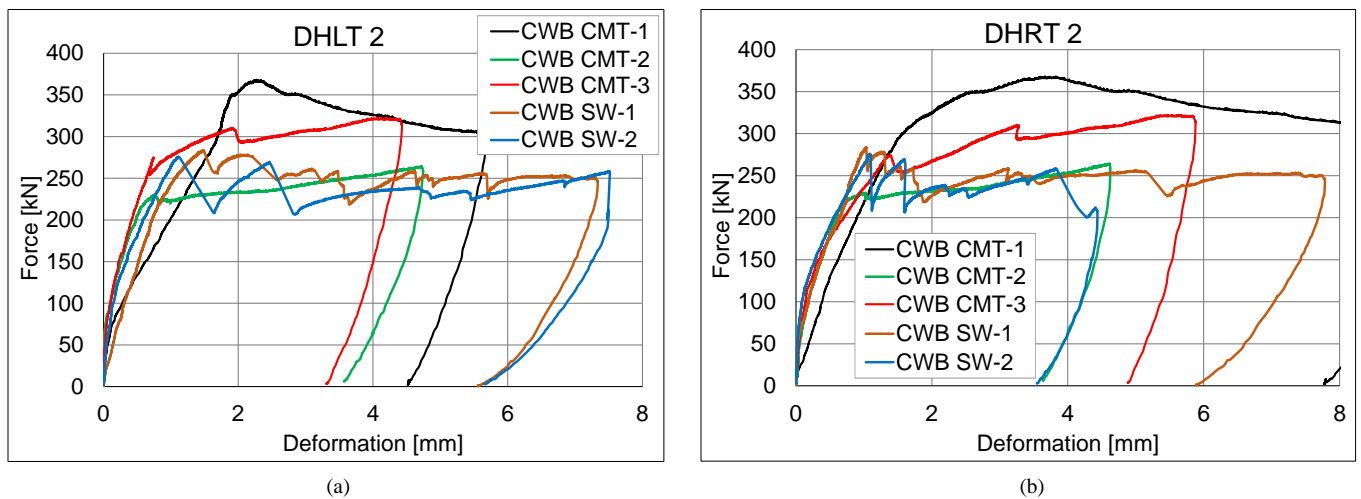


Figure 17. Slippages and deformations of the backward top connection between the flanges and the support: a) left side, b) right side

Figures 16 and 17 show the response of the top connection between the flanges and the support device. Of course, the direction of the displacement is opposite the bottom connection, but for ease of graph comparison, the numerical values have the same sign. The first observation concerns the initial slope of the curve. The force value for which the slippage starts to develop is similar in most cases but quite different for the frontal right top connection (Figure 16-b). The cause of the development of the slip may be the preload of the bolt. The bolt tightening was performed manually, resulting in a different initial capacity of the connection.

Regarding the deformations of the connections, the values from which the plastic deformations occur are very similar for the positions. The value is approximately between 0.5 and 1 mm, which represents the tolerance between the bolts and the holes in the assembly. A larger deformation develops for the SW beams, which can be related to the less rigid behaviour provided by the spot welds compared to the brazed throats.

As mentioned, a tolerance of 1 mm was considered for the M12 bolts that connect the beam parts to the support device. The final values recorded by the transducers are much larger. The plastic deformations of the bolt holes, observed after testing, partly explain the recorded values (see Figure 18). Also, the direction of the hole deformation does not follow the theoretical stress direction, i.e., the flanges are subjected to normal stresses and the shear panels are subjected to tangential stresses. The final deformation of the holes shows a combination of the internal forces.

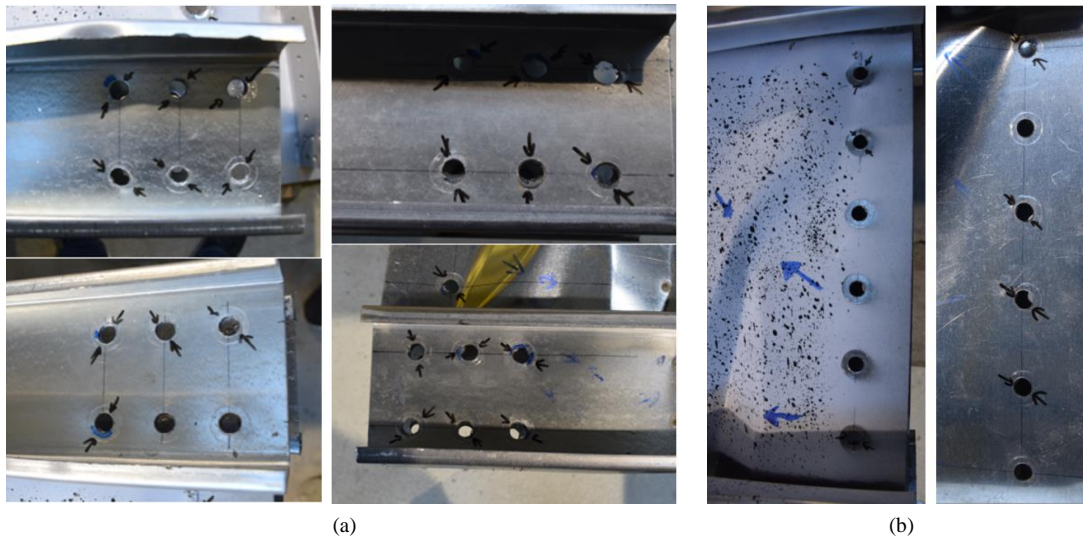


Figure 18. Deformations of bolt holes: a) in the flange, b) in the shear panel

### 3.1.3. Base Material

The mechanical properties of the base material are presented in Figure 19. Different yield limits were obtained for different thicknesses, as presented in Table 1.

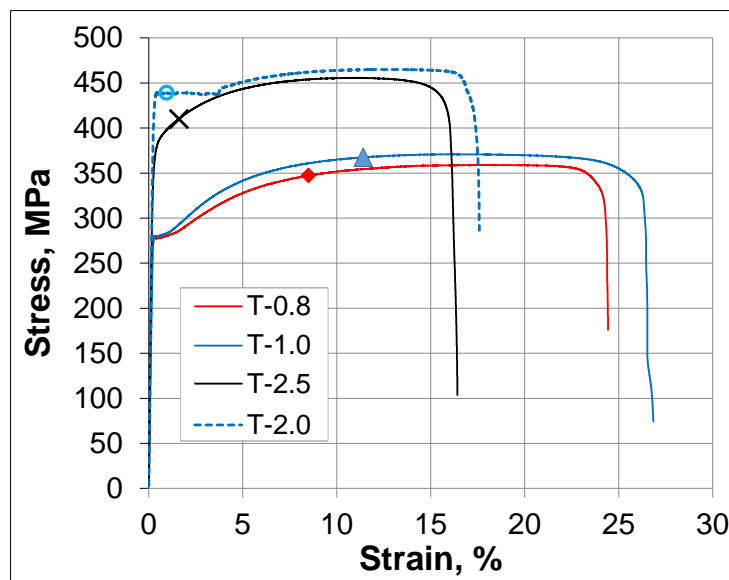


Figure 19. Stress-strain relationships for base material

Table 1. Material properties

| Sheet thickness (mm) | $R_{p0.2}$ (MPa) | $R_m$ (MPa) | $A_{gt}$ % | $A_t$ % |
|----------------------|------------------|-------------|------------|---------|
| 0.8                  | 279.64           | 361.76      | 18.41      | 26.60   |
| 1.0                  | 281.33           | 373.50      | 16.70      | 26.14   |
| 1.2                  | 366.82           | 420.68      | 13.15      | 19.83   |
| 2.0                  | 431.78           | 464.46      | 11.79      | 19.70   |

where  $R_{p0.2}$  stress at 0.2% is strain,  $R_m$  is stress corresponding to the maximum force,  $A_{gt}$  is total extension at maximum force, and  $A_t$  is total extension at the moment of fracture

## 3.2. Finite Element Analysis

### 3.2.1. Validation of the FE Model

The numerical model for the beam leads to the force-displacement curve showing a good correlation with the experimental results, as shown in Figure 20.

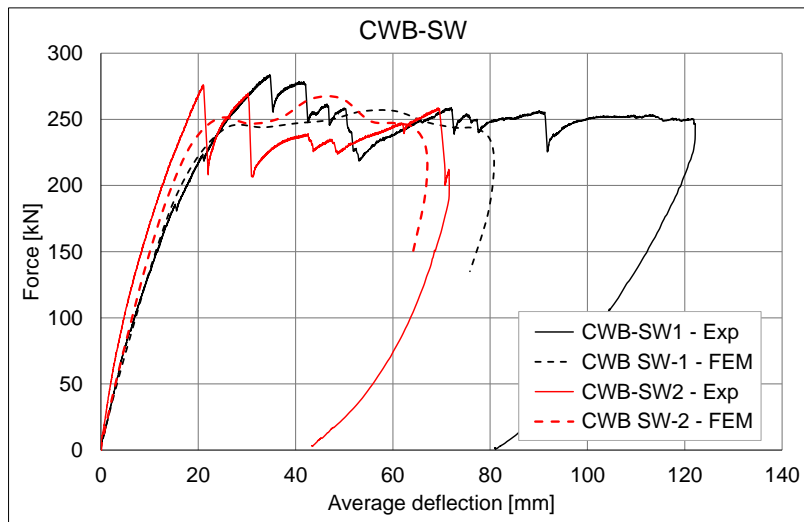


Figure 20. Experimental and numerical results for the beam

A visualization in the form of maximum principal stresses can be observed in Figure 21-a, for the shell element model, and in Figure 21-b, for the 3D element model, of the bolted connection of the beam. Plasticization of the material is produced for most holes, but more severely for the holes in the lipped channels of the flanges, especially the top flange where the catenary effect of the shear panel appears. Also, it is observed that most of the strains are concentrated in the first column of the bolt array.

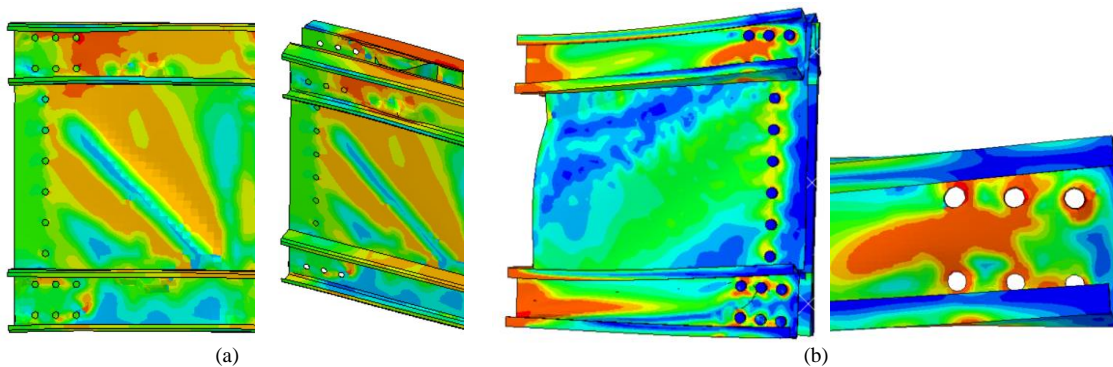


Figure 21. Stress distribution in the parts of the bolted connection: a) shell elements model, b) 3D elements model

The results for the connection using solid elements, the slippage in the top flange, are similar between the experimental and finite element analysis, as presented in Figure 22. The end plate of the connection was not modelled because the rigidity of the connection depends on its thickness, and the design thickness depends on the column profile.

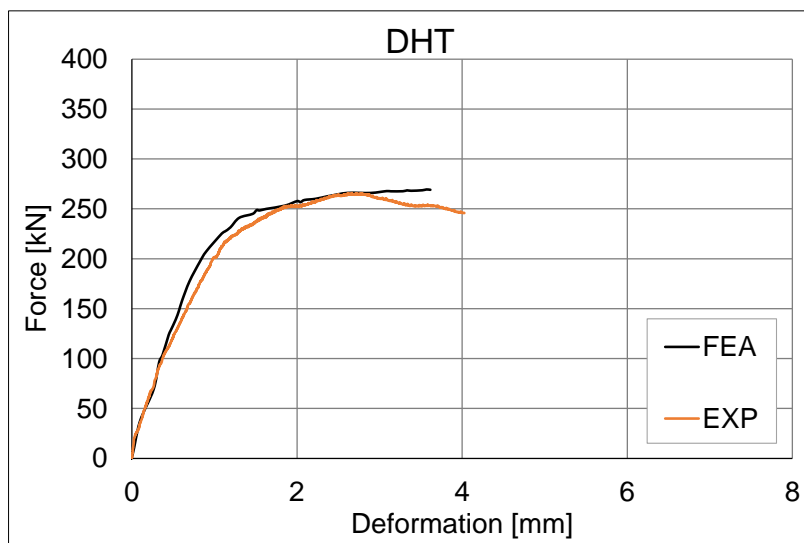


Figure 22. Slippage comparison between experimental and finite element analysis of the bolted connection

### 3.2.2. Connection Alternative Solutions

A first solution to optimise the connection (SOL1) is to transfer the shear force to the lipped channel profile web. Due to the relatively high height of the beam, the lever arm between the flanges leads to small axial forces, and by reducing the length between the fixing point of the flanges, instability problems are avoided, allowing the shear force to be resisted. In this manner, a model was created in which the bolts of the shear plates were removed and a strut, consisting of a 2 mm thick cold-formed profile, was fixed at the limit between the shear panels and the bolted connection, as Figure 23 shows.

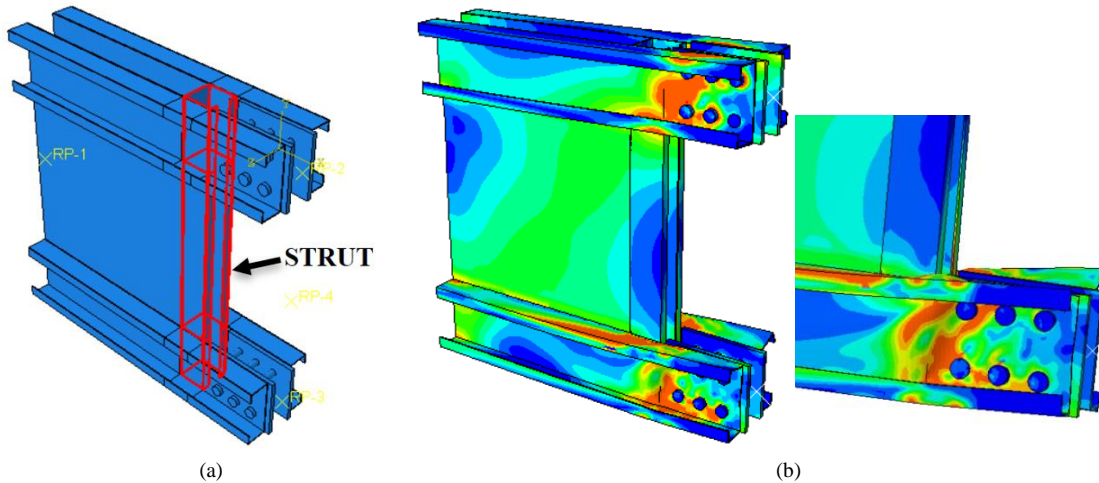


Figure 23. SOL1 a) Configuration, b) Deformation and stress distribution

The strut was considered to be tied in both extreme parts of each lipped channel web. This solution will transmit the shear force from the beam to the connection only through the web of the lipped channel profiles.

From the deformed shape presented in Figure 23-b, local buckling of the lipped channel web between the strut and the bolted connection and distortional buckling along the bolted connection are observed.

Thus, to eliminate the instability in the bolted connection length, two bolts were added to each flange of the lipped channels. Furthermore, because small stresses were developed in the last column of the bolted connection, to optimise material consumption, only two bolt columns were considered in the web of the lipped channels for the second solution SOL2, as shown in Figure 24-a. A high concentration of deformations and deformations is visible mainly in the compressed bottom flange (see Figure 24-b), which requires a stronger configuration of the beam end connection.

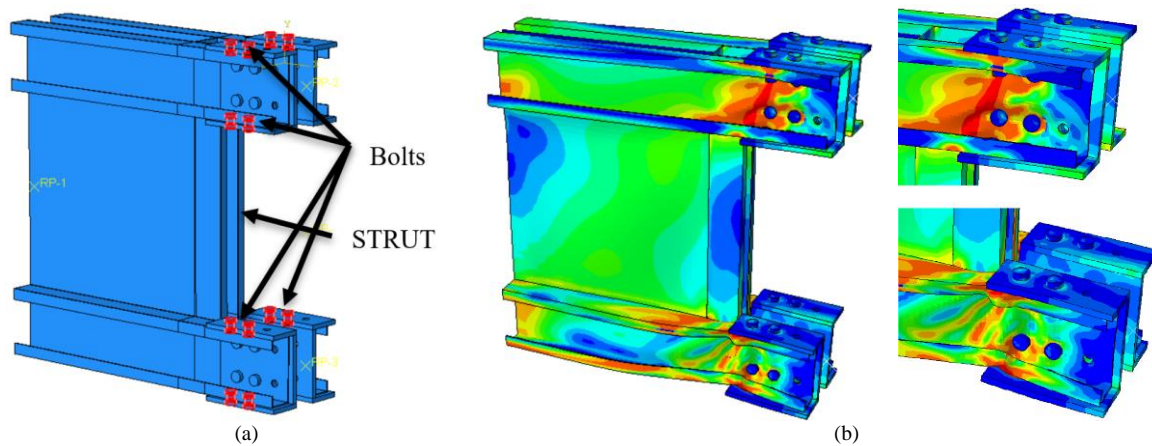


Figure 24. SOL2 a) Configuration, b) Deformation and stress distribution

An assembly of welded Rectangular Hollow Sections (RHS120×60×5) was defined to increase the rigidity of the end of the beam (SOL3), as presented in Figure 25-a. Bolts are used only for the flanges, while brazing of the thin shear panels to the vertical RHS can be used to limit the shear panel deformation. Also, on the common edges, the flange can be connected to the vertical RHS by brazing. In Figure 25-b, the stress distribution and deformation of the connection qualitatively show an improvement in the joint, avoiding a deformation concentration as seen for SOL2. Deformations of the holes are still visible in the beam flanges, as can be seen in the detail of Figure 25-b.

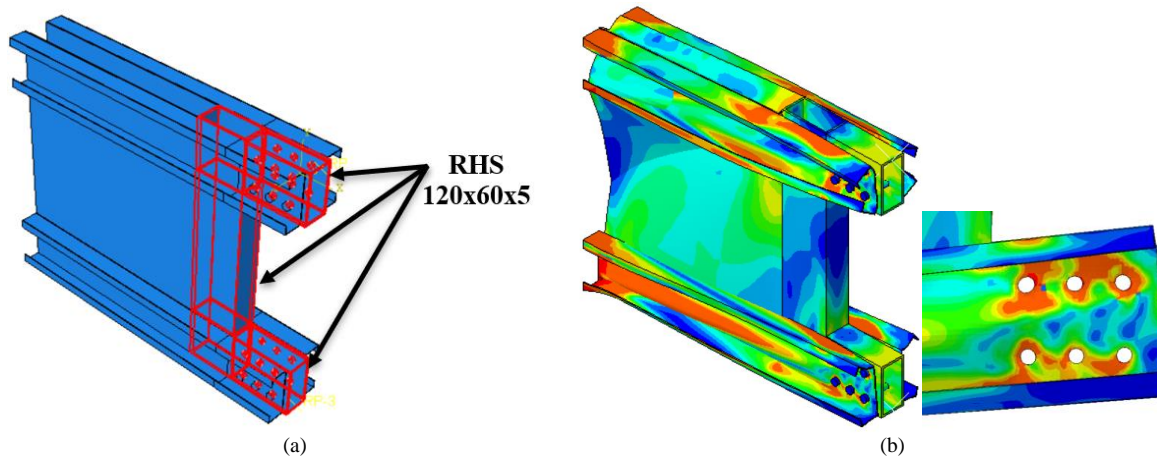


Figure 25. SOL3 a) Configuration, b) Deformation and stress distribution

Although the rigidity of the assembly in SOL3 is greater than in the previous solutions, to reduce the effect of the shear panel, a truss assembly of RHS profiles was considered as a substitute for the entire beam end (SOL4), as shown in Figure 26-a. Of course, the maximum stresses are relocated to the connection between the CWB and the welded RHS assembly (close to the vertical strut) as the rigidity of the assembly is greater than that of the shear panels, which are prone to instability.

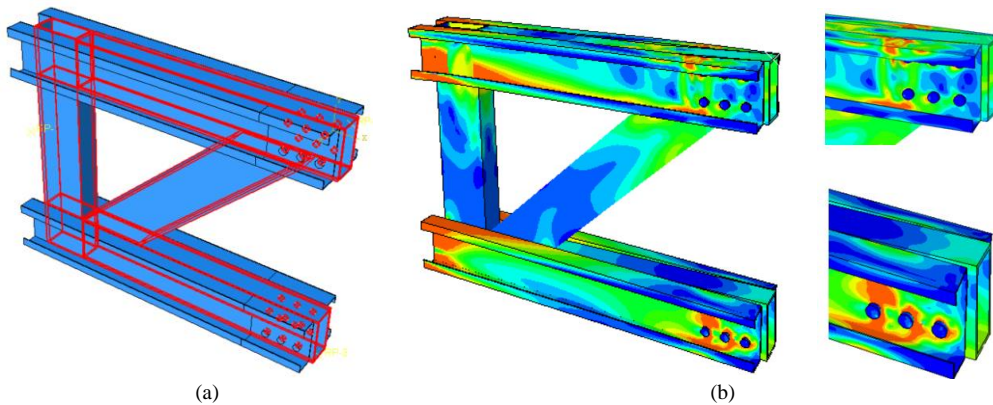


Figure 26. SOL4 (a) Configuration, (b) Deformation and stress distribution

Quantitatively, the response of the proposed connection configurations is presented in Figure 27-a for the top connection and in Figure 27-b for the bottom connection.

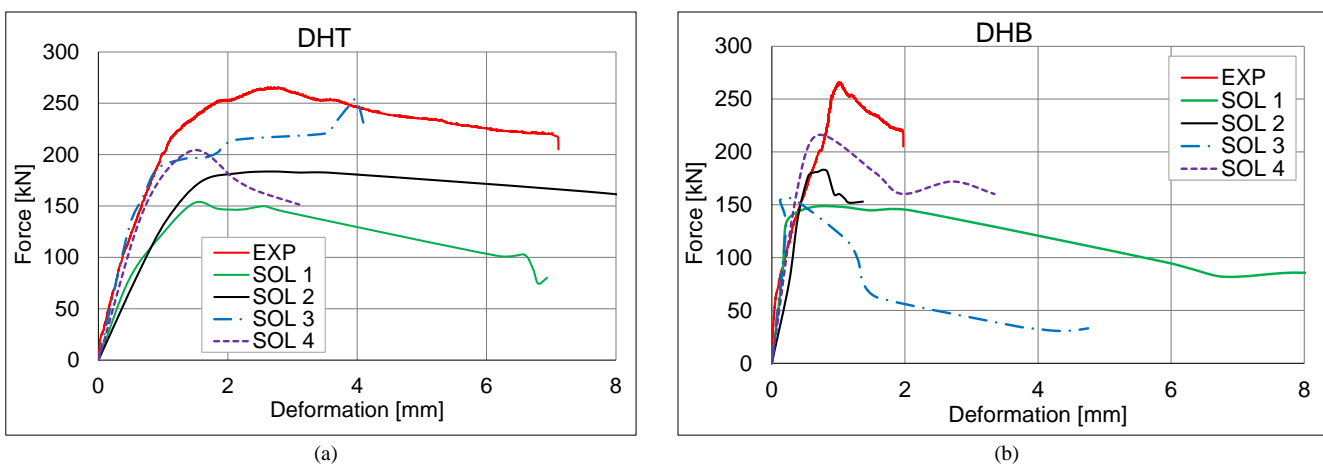


Figure 27. Slippages and deformations of the frontal top connection between the flanges and the support: a) left side, b) right side

For the tensioned part, the top flange, the proposed solutions can lead to a smaller or bigger rigidity, while for the compressed connection, the rigidity is very similar to the one in the experiment. Nevertheless, the compression in the elements leads to a smaller capacity caused by the instabilities of the cold-formed elements.

## 4. Discussions

The built-up cold-formed steel corrugated web beams represent an efficient solution for structural elements as they offer high rigidity and capacity with respect to material consumption. In addition to the response of the beams, the connection also represents a decisive factor for the overall response of the structure. From the experimental data, the designed connection offers good capacity, the connection reaching the tolerance of the bolt holes (1 mm) at a force level in the range of the yielding force. Except DHCT recordings, which represent the deformation of the end plate of the connection and depend on the thickness of the plate and the T-stub configuration, the connections between the lipped channel profiles and the steel plates responded similarly in the plastic range, except for the CMT-1 and CMT-3. These beams were subjected to the greatest forces applied to the beam specimens.

Slightly increased deformations appeared in the top connections (DHT) compared to the bottom connections (DHB). The cause of the differences is explained by the behaviour of the shear panel, which, due to its thin gauge, transmits the load only to the upper connection, as observed in Figure 21. Moreover, as the deflection of the beam increased, the connection response also became plastic, thus the need to provide a more rigid area before the connection between the flange and the support device.

SOL1 and SOL2 have good resistance and ductility, but SOL3 and SOL4 have the advantage of increased rigidity. For the compressed part of the connection, the rigidity is similar for all four configurations; the greatest resistance is provided by the welded RHS assembly that replaces the shear panels of the CWB. As resulted from Papargyriou et al. [14], the current study also shows that engaging the flanges of the lipped channels to the load transfer, increases the capacity of the connection, by comparing SOL1 and SOL2. Due to the distribution of forces from the shear panel to the two flanges, the response of the entire connection must be characterised separately by the response of the top and bottom connection. The connection subjected to compression shows a higher rigidity, it is loaded rapidly but it cannot reach its full capacity due to instability of the compressed thin cold-formed elements, see Table 2. The same response of the connection was observed for the deformed shape of the tested specimen by Papargyriou et al. [14].

**Table 2. Connection response**

| Solution | TOP                   |           |         | BOTTOM                |          |         |
|----------|-----------------------|-----------|---------|-----------------------|----------|---------|
|          | F <sub>max</sub> (kN) | K (kN/mm) | Ductile | F <sub>max</sub> (kN) | K (N/mm) | Ductile |
| Exp      | 265.9                 | 206.2     | Yes     | 265.9                 | 276.4    | No      |
| SOL1     | 152.8                 | 124.7     | Yes     | 148.1                 | 571.4    | Yes     |
| SOL2     | 183.6                 | 129.2     | Yes     | 183.1                 | 348.7    | No      |
| SOL3     | 253.0                 | 230.8     | Yes     | 154.7                 | 510.2    | No      |
| SOL4     | 203.9                 | 206.9     | Yes     | 215.9                 | 454.5    | No      |

## 5. Conclusion

The connections of built-up, cold-formed CWB usually require a large number of bolts due to the small thickness of the cold-formed profiles. Due to the deformation of the shear panels of the CWB, the forces transferred to the connection are not evenly distributed. To equilibrate the forces transmitted to the bolted flange connections and eliminate the bolts for the shear force transmitted by the shear panels, four configurations were analysed. The four proposed configurations represent a suitable solution for the CWB connections, but their capacity is limited by the instability of the cold-formed lipped channel profile.

Several solutions can be adopted for the connection of CWBs with a rigidity similar to the one offered by the bolted connection used in the experiment, as presented in the current study. Solutions for reducing the number of bolts (SOL3) can be obtained while maintaining the same rigidity and reaching high capacities.

As the response of the connection in tension is different from the response in compression, the response to cyclic loading must be further studied. More studies will be conducted within a new research project under development. Standardised connection joints will be proposed. Thereupon, real-scale tests will be performed on several connection typologies and full-scale frames considering the proposed connection joints and the results from this parametric study.

## 6. Declarations

### 6.1. Author Contributions

Conceptualization, I.B. and V.U.; methodology, V.U.; software, I.B.; validation, I.B.; formal analysis, V.U. and M.B.; investigation, V.U., M.B., S.B. and I.B.; resources, I.B.; data curation, V.U. and I.B.; writing—original draft preparation, I.B.; writing—review and editing, V.U. and I.B.; visualization, V.U.; supervision, V.U.; project administration, V.U. and I.B.; funding acquisition, I.B. All authors have read and agreed to the published version of the manuscript.

## 6.2. Data Availability Statement

The data presented in this study are available on request from the corresponding author.

## 6.3. Funding

The research was financed by “Internal program for stimulating and rewarding the teaching activity” 2021, Politehnica University of Timisoara, Romania, contract no. 10165/11.06.2021.

## 6.4. Conflicts of Interest

The authors declare no conflict of interest.

## 7. References

- [1] Wu, Y., Du, X., & Yuan, H. (2021). Structural performance of cold-formed steel box girders with C-section flanges and sinusoidal corrugated webs. *Structures*, 34, 4851–4866. doi:10.1016/j.istruc.2021.10.066.
- [2] Wu, Y., Du, X., Yuan, H., & Zhou, M. (2022). Shear behaviour and design of cold-formed steel box girders with tubular flanges and sinusoidal corrugated webs. *Thin-Walled Structures*, 174, 109066. doi:10.1016/j.tws.2022.109066.
- [3] Selvaraj, S., & Madhavan, M. (2021). Design of Cold-Formed Steel Back-To-Back Connected Built-up Beams. *Journal of Constructional Steel Research*, 181, 106623. doi:10.1016/j.jcsr.2021.106623.
- [4] Dubina, D., Ungureanu, V., & Gîlia, L. (2015). Experimental investigations of cold-formed steel beams of corrugated web and built-up section for flanges. *Thin-Walled Structures*, 90, 159–170. doi:10.1016/j.tws.2015.01.018.
- [5] Lukačević, I., Ćurković, I., Rajić, A., & Bartolac, M. (2022). Lightweight Composite Floor System - Cold-Formed Steel and Concrete - LWT-FLOOR Project. *Buildings*, 12(2). doi:10.3390/buildings12020209.
- [6] Pedreschi, R. F., & Sinha, B. P. (2008). An experimental study of cold formed steel trusses using mechanical clinching. *Construction and Building Materials*, 22(5), 921–931. doi:10.1016/j.conbuildmat.2006.12.014.
- [7] Dubina, D., & Zaharia, R. (1997). Cold-formed steel trusses with semi-rigid joints. *Thin-Walled Structures*, 29(1–4), 273–287. doi:10.1016/s0263-8231(97)00028-1.
- [8] Sangeetha, P., Revathi, S. M., Sudhakar, V., Swarnavarshini, D., & Sweatha, S. (2020). Behaviour of cold-formed steel hollow beam with perforation under flexural loading. *Materials Today: Proceedings*, 38, 3103–3109. doi:10.1016/j.matpr.2020.09.492.
- [9] Jiao, P., Borchani, W., Soleimani, S., & McGraw, B. (2017). Lateral-torsional buckling analysis of wood composite I-beams with sinusoidal corrugated web. *Thin-Walled Structures*, 119, 72–82. doi:10.1016/j.tws.2017.05.025.
- [10] EN 1993-1-8. (2005). Design of steel structures - Part 1-8: Design of joints. European Committee for Standardization (CEN), Brussels, Belgium.
- [11] EN 14399-1:2015. High-strength structural bolting assemblies for preloading. Part 1: General requirements. European Committee for Standardization (CEN), Brussels, Belgium.
- [12] Dubina, D., Stratan, A., Ciutina, A., Fulop, L., & Nagy, Zs. (2004). Performance of ridge and eaves joints in cold-formed steel portal frames. *Proceedings of the 17<sup>th</sup> International Specialty Conference*, 4-5 November, 2004, Orlando, United States.
- [13] Mojtabaei, S. M., Becque, J., & Hajirasouliha, I. (2021). Behavior and Design of Cold-Formed Steel Bolted Connections Subjected to Combined Actions. *Journal of Structural Engineering*, 147(4), 4021013. doi:10.1061/(asce)st.1943-541x.0002966.
- [14] Papargyriou, I., Mojtabaei, S. M., Hajirasouliha, I., Becque, J., & Pilakoutas, K. (2022). Cold-formed steel beam-to-column bolted connections for seismic applications. *Thin-Walled Structures*, 172, 108876. doi:10.1016/j.tws.2021.108876.
- [15] Ye, J., Mojtabaei, S. M., & Hajirasouliha, I. (2019). Seismic performance of cold-formed steel bolted moment connections with bolting friction-slip mechanism. *Journal of Constructional Steel Research*, 156, 122–136. doi:10.1016/j.jcsr.2019.01.013.
- [16] Fahmy, A. S., Swelem, S. M., & Musstaf, H. H. (2020). Beam-Column Connections Behavior of Cold-Formed Steel Members: New Experimental Configuration. *KSCE Journal of Civil Engineering*, 24(7), 2147–2159. doi:10.1007/s12205-020-2009-7.
- [17] Hanna, M., El-Saadawy, M., El-Mahdy, G., & Aly, E. (2018). Behavior of Beam to Column Cold-Formed Section Connections Subjected to Bending Moments. *Proceedings of the International Specialty Conference on Cold-Formed Steel Structures*, 7-8 November, 2018, St. Louis, United States.
- [18] ElSabbagh, A., Sharaf, T., Nagy, S., & ElGhandour, M. (2019). Behavior of extended end-plate bolted connections subjected to monotonic and cyclic loads. *Engineering Structures*, 190, 142–159. doi:10.1016/j.engstruct.2019.04.016.
- [19] Nagy, Z., Gîlia, L., & Neagu, C. (2017). Experimental investigations of cold-formed joints for multi-storey steel framed structures. *Proceedings of the Romanian Academy*, 18(3), 256-264.

- [20] Rinchen, & Rasmussen, K. J. R. (2019). Behaviour and modelling of connections in cold-formed steel single C-section portal frames. *Thin-Walled Structures*, 143, 106233. doi:10.1016/j.tws.2019.106233.
- [21] Bondok, D. H., & Salim, H. A. (2017). Failure capacities of cold-formed steel roof trusses end-connections. *Thin-Walled Structures*, 121, 57–66. doi:10.1016/j.tws.2017.09.026.
- [22] Lukačević, L., Krolo, P., & Bakran, A. (2022). Experimental Investigation of Novel Angle Bracket Connection in Cold-Formed Steel Structures. *Buildings*, 12(8), 1115. doi:10.3390/buildings12081115.
- [23] Deng, E. F., Lian, J. Y., Liu, Z., Zhang, G. C., Wang, S. B., & Cao, D. Bin. (2022). Compressive Behavior of a Fully Prefabricated Lifiable Connection for Modular Steel Construction. *Buildings*, 12(5), 649. doi:10.3390/buildings12050649.
- [24] Lacey, A. W., Chen, W., Hao, H., & Bi, K. (2019). Review of bolted inter-module connections in modular steel buildings. *Journal of Building Engineering*, 23, 207–219. doi:10.1016/j.job.2019.01.035.
- [25] European Commission. (2017). INNO3DJOINTS: Innovative 3D joints for economic and robust hybrid tubular construction. Research Project, European Commission, Brussels, Belgium.
- [26] Poursadrollah, A., D’Aniello, M., De Martino, A., & Landolfo, R. (2020). Preliminary study on the seismic performance of hybrid steel structures with truss lightweight girders and plug-and-play connections. *Ingegneria Sismica*, 37(1), 102–114.
- [27] Simões da Silva, L., Silva, L. C., Tankova, T., Craveiro, H. D., Simões, R., Costa, R., D’Aniello, M., & Landolfo, R. (2021). Performance of modular hybrid cold-formed/tubular structural system. *Structures*, 30, 1006–1019. doi:10.1016/j.istruc.2021.01.066.
- [28] Ungureanu, V., Both, I., Burca, M., Radu, B., Neagu, C., & Dubina, D. (2021). Experimental and numerical investigations on built-up cold-formed steel beams using resistance spot welding. *Thin-Walled Structures*, 161, 107456. doi:10.1016/j.tws.2021.107456.
- [29] Both, I., Ungureanu, V., Tunea, D., Crisan, A., & Grosan, M. (2018). Experimental and numerical investigations on cold-formed steel beams assembled by MIG brazing. *Proceedings of the International Conference on Engineering Research and Practice for Steel Construction*, 5-7 September, 2018, Hong Kong, China.
- [30] ISO 6892-1:2016. (2016). *Metallic materials – Tensile testing – Part 1: Method of test at room temperature*. International Organization for Standardization, Geneva, Switzerland.
- [31] ABAQUS Software. (2014). *ABAQUS/CAE User’s Manual 6.14*; Dassault Systèmes Simulia Corp. Massachusetts, United States.
- [32] EN 1993-1-5:2006. *Eurocode 3: Design of steel structures - Part 1-5: Plated structural elements*. European Committee for Standardization (CEN), Brussels, Belgium.